High-resolution observations of internal wave induced turbulence in the deep ocean

Hans van Haren

Royal Netherlands Institute for Sea Research (NIOZ)

hans.van.haren@nioz.nl

Abstract

An overview is presented of high-resolution temperature (T) observations above underwater topography in the deep, stably stratified ocean. The Eulerian mooring technique is used to monitor T-variations with typically 100 sensors distributed over lines between 40 and 400 m long. The independent sensors sample at a rate of 1 Hz for up to one year with a precision better than 0.1 mK. Under conditions of a tight T-salinity (T-density) relationship, the temperature data are used to quantify turbulent overturns. These observations show two distinctive turbulence processes that are associated with different phases of a large-scale (mainly tidal) internal gravity wave: i) highly nonlinear turbulent bores during the upslope propagating phase, and ii) Kelvin-Helmholtz billows, at some distance above the bottom, during the downslope phase. Both convective turbulence following Rayleigh-Taylor instabilities and shear-induced instabilities are observed with internal waves breaking. With a newly developed five-lines (3D-)mooring, the transition from isotropy (full turbulence) to anisotropy (stratified turbulence/internal waves) is revealed.

1 Introduction

The sampling of spatial scales of 1 m, over a range of about 100 m, and temporal scales of 1s, over months, are sufficient to observe in detail the large, energy containing turbulent eddies and all of the internal waves and their breaking above underwater topography in the ocean. Underwater wave breaking is thought the key mechanism for the redistribution of nutrients and heat (to maintain the ocean stratified in density, Munk 1966; Armi, 1978), and the resuspension of sediment.

The ocean in general, but near the surface and above underwater topography in particular, is thus turbulent that the Reynolds number is large (10^4-10^6). Such an environment is hard to achieve in the laboratory, especially considering scales larger than a few meters. Not only are Reynolds numbers large in the vicinity of ocean topography, the turbulent mixing is likely to be efficient because of the rapid re-stratification. Under both these conditions and a locally tight T-density relationship, data from a sufficiently large array of high-resolution T-sensors can be used to estimate turbulence dissipation rate (like the heat flux) and eddy diffusivity using the method of reordering vertical profiles in statically stable ones (Thorpe, 1977; 1987). The thus obtained overturning scales are a measure for the largest turbulent scales in stratified turbulence, the Ozmidov scales, to within one order of magnitude (Dillon, 1982). The eddy diffusivity is calculated under the assumption of a constant mixing efficiency of 0.2, as was empirically established for turbulent near-surface conditions (Oakey, 1982).

2 Instrumentation

The Eulerian moored 'NIOZ4' are self-contained T-sensors developed at the Royal Netherlands Institute for Sea Research, NIOZ (van Haren et al., 2009). They sample at a rate of 1 Hz, with precision better than 0.5 mK (after drift-correction) and a noise level of <0.1 mK. Typically, 100-200 sensors are attached to a mooring line which varies between 50 and 400 m in length. Every four hours, all sensors are synchronized via induction to a single standard clock, so that the entire range is sampled in less than 0.02 s. This, together with the relatively small mooring deflection due to 300-400 kg net buoyancy, implies a near-instantaneous and near-vertical 'synoptic' view which is not achievable via free-falling or lowered ship-borne instrumentation. A typical advection speed of 0.1 m s^{-1} causes a horizontal deflection of <1 m half-way the T-sensor array compared to lowest and uppermost sensors. Such displacement is less than a factor of 10 smaller than, 1/ the bottom slope, 2/ fictitious displacements associated sampling strategies like shipborne Conductivity-Temperature-Depth 'CTD' or free-falling microstructure profiler. Such instruments take 400-600 s to cross the range of moored T-sensors at standard vertical speeds by which structures measured at the depth of the uppermost T-sensor have been displaced horizontally by several 10s of meters compared with those measured at the lowest T-sensor. The moored T-data are converted into 'Conservative' (~potential) Temperature data Θ (IOC, SCOR, IAPSO, 2010). They are used as tracer for density anomaly (σ_x) variations following the relation $\delta\sigma_x = \alpha\delta\Theta$, where α denotes the apparent thermal expansion coefficient under local conditions (x indicates the reference depth in km). This relation is established using data around the range of moored sensors from shipborne CTD-profiles, preferably obtained within 1 km from the mooring site.

3 Observations

In the open ocean, tidal and high-frequency internal wave motions appear as smooth, linear waves which keep the ocean interior in persistent motion, with typical amplitudes reaching several tens of meters (Fig. 1). The weakly turbulent motions are smooth, not perfectly sinusoidal in shape, and have relatively large vertical coherent scales with near-zero phase difference over the 130 m range of sensors ("local vertical mode-1"), at both tidal and near-buoyancy frequencies. Thickness of strongly stratified layers drops below sensor separation, in this case 2.5 m, while weakly stratified layers can exceed half the sensor range. Turbulent overturns are few and far apart, despite the 1-Hz sampling. However, due to the ill-defined T-density relation, which varies in time and space with water masses under intermediate Mediterranean Sea influence, quantification of turbulence parameters is difficult. Such estimates are made using limited conventional CTD-observations at stations nearby which provide average values of $\varepsilon \approx 10^{-9}$ m^2 s^{-3} and K_z = 2-3×10^{-5} m^2 s^{-1} over the range of the thermistors. These values correspond with upper (<2000 m) open ocean microstructure observations (e.g., Gregg, 1989).
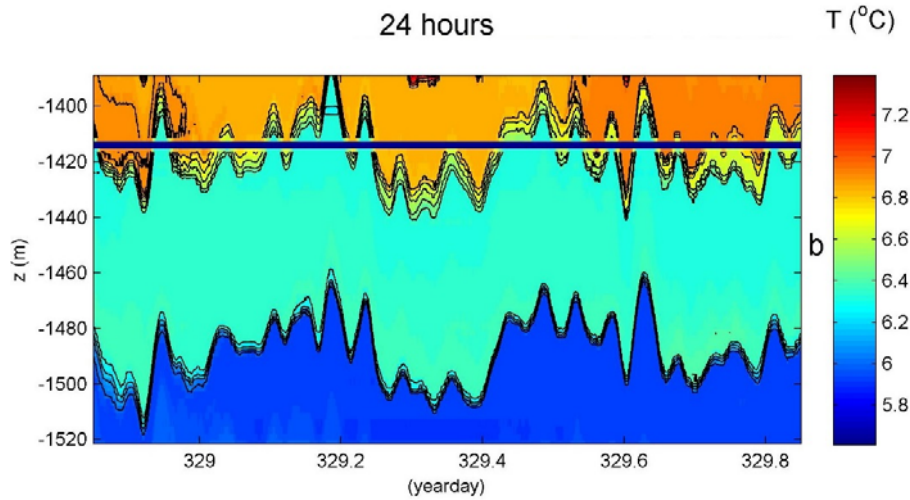
Figure 1: One day detail example of open ocean internal wave motions observed using 54 NIOZ3 sensors at 2.5 m vertical intervals. The sensors were below the top-buoy of a 3800 m long mooring in the Canary Basin NE Atlantic Ocean. The horizontal line indicates a failing sensor. In black, isotherms every 0.1°C. Some influence of Mediterranean water is visible in apparent T-inversion layers: e.g., in the ranges [1410, 1420] m and [1460, 1480] m.

Much more turbulent are internal wave motions near topography, although their intensity is found to be dependent on slope steepness. Although bottom slopes are on average just a few per cent and typical internal tide generating horizontal currents are 0.1 m s^{-1}, the impact of such currents and slopes is spectacular in their production of wave breaking in the near-interior. Turbulent upslope propagating bores range from 10 to 100 m vertical scales (Fig. 2) and dominate sediment resuspension involving local vertical currents with amplitudes O(0.1) m s^{-1} (Hosegood et al., 2004). Turbulent dissipation rates reach $\varepsilon = 10^{-5}$-10^{-4} m^2 s^{-3}, eddy diffusivity $K_z = 10^{-1}$-10^0 m^2 s^{-1}. The front itself is the only large overturn extending from the bottom upward.
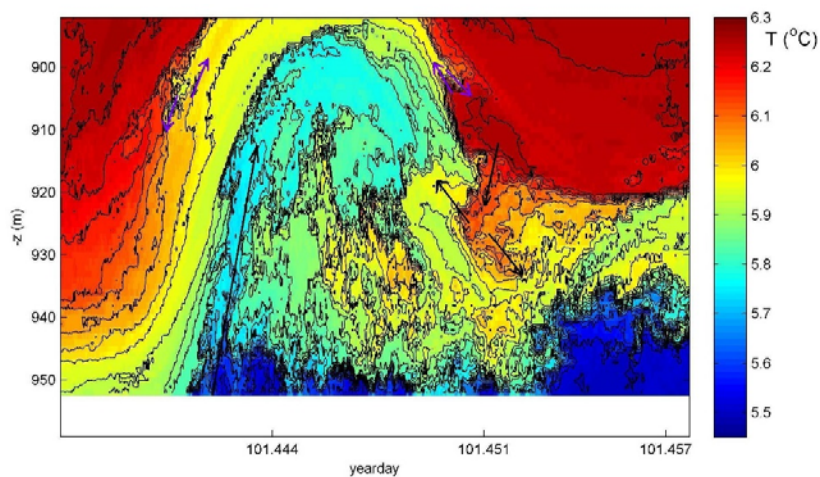

Figure 2: Half hour detail example of upslope propagating bore motions observed using 60 NIOZ4 sensors at 1.0 m vertical intervals south of New Zealand.

VIIIth Int. Symp. on Stratified Flows, San Diego, USA, Aug. 29 – Sept. 1, 2016

The turbulent heat flux (and ε) are largest at the frontal bore, and relatively smaller in the weakly stratified large convective overturns preceding it where K_z is largest. These large interior overturns are associated with relatively large downward motions originating from above. This downdraught seems part of the turbulent bore moving up the slope. The front is sharpened when the interior overturns just preceding it are large and more intense. Averaged over time, over a two-week spring-neap period, and over depth, over the range of thermistors O(100 m), gives $\langle\varepsilon\rangle \approx 10^{-7}$ m^2 s^{-3}, $\langle K_z\rangle = 3\pm1\times10^{-3}$ m^2 s^{-1}. These mean 'sloping topography' values are 100 times larger than observed open ocean values.
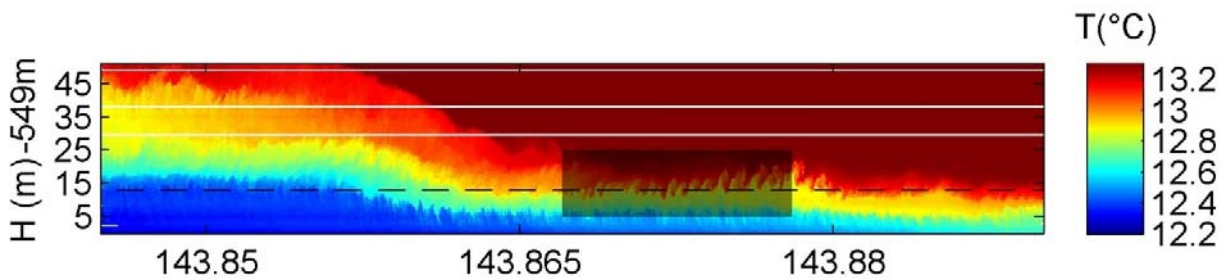

Figure 3: One hour detail example of downslope propagating, warming phase of the internal tide observed using 100 NIOZ3 sensors at 0.5 m vertical intervals near the top of Great Meteor Seamount, NE Atlantic Ocean.

Above sloping topography not only large overturns are observed associated with a frontal bore, but also bursts are found of smaller overturns throughout a tidal period (Fig. 3). For example, during the warming tidal phase, turbulence mainly occurs in the stratified waters well away from the bottom in patches of typically 1-10 m thickness and of 30-300 s duration. They are part of high-frequency overturning Kelvin-Helmholtz shear instabilities (van Haren and Gostiaux, 2010). These instabilities are indirectly associated with the large-scale inertial-tidal shear, and with the smaller near-N internal waves that often appear in a local vertical mode-2 fashion. In the O(1-10 m) high turbulence patches away from the bottom, peak turbulence parameter values are $\varepsilon = 10^{-6}$-10^{-5} m^2 s^{-3}, $K_z = 10^{-3}$-10^{-1} m^2 s^{-1}. Much rarer are ocean observations such as off New Zealand on Holmboe instabilities, overturning of interfacial (thin stratified) layer internal waves. Largest turbulence is generated by 25 m high asymmetric Holmboe overturns (van Haren, 2015).

It appears unlikely that tides govern internal wave turbulence in seas like [most of] the Mediterranean and the Baltic. There, the dominant low-frequency internal waves are near-inertial waves. In the deep Mediterranean around 4000 m, variations in temperature are so weak, that analysis can only be made relative to the local adiabatic lapse rate. A relative ΔT-image has a range of ±0.0015°C, within which all meso-, inertial- and small-scale variability occurs (van Haren and Gostiaux, 2011). Non-traditional inertial frequency (f) waves govern turbulent overturning and have O(1) = $|w_f|/|u_f|$ aspect ratio, and their vertical currents $|w_f| \leq 2.5\times10^{-2}$ m s^{-1} are relatively large, commensurate the vertical isotherm excursions exceeding 200 m (peak-trough).

4 Discussion

Underwater topography like seamounts causes the breaking of large 'internal waves' with associated turbulent mixing strongly affecting the redistribution of sediment. Here, ocean-turbulence is characterized and quantified in the lowest 100 m of the water column. At four nearby sites above the slope of a deep-ocean seamount the moored T-sensors show very different turbulence generation mechanisms over 3 and 5 km horizontal separation distances (van Haren et al., 2015). At the steepest slope, turbulence was 100-times more energetic than at the shallowest slope where turbulence was still more energetic than found in the open-ocean, away from topography. The turbulence on this extensive slope is caused by slope steepness and nonlinear wave evolution, but not by bottom-friction, 'critical' internal tide reflection or lee-wave generation.

One 400-m long line was moored at a site with bottom slope being supercritical for semidiurnal internal tides by a factor of two. The observations show a gradual decrease in turbulence parameters by one order of magnitude (when averaged over a day or longer) over a vertical distance of 250 m, upwards from 150 m above the bottom. These findings compare well with previous observations from coarser sampled arrays (e.g., Aucan et al., 2006; Levine and Boyd, 2006) and recent high-resolution numerical modelling (Winters, 2015; Sarkar, pers. comm., 2016). They stress the importance of internal wave breaking for the ocean as a whole. Extrapolating, it needs to be investigated how stable the present balance is between internal waves, shear and stratification, in view of potential increase in ocean heat storage. On the smaller scales, we need more modeling and observational efforts to establish turbulence processes in full three-dimensions 3D, instead of present 1D or 2D, at best.

First measurements using a unique small-scale 3D mooring array consisting of five parallel lines, 100 m long and 4 m apart and holding up to 550 high-resolution T-sensors, provided details of the inertial subrange. Vertical and horizontal coherence spectra show an aspect ratio of 0.25-0.5 near the buoyancy frequency, evidencing anisotropy. At higher frequencies, the transition to isotropy (aspect ratio of 1) is found within the inertial subrange. Above the continuous turbulence spectrum in this subrange, isolated peaks are visible that locally increase the spectral width, in contrast with open-ocean spectra. Their energy levels are found to be proportional to the tidal energy level.

References

Armi, L. (1978). Some evidence for boundary mixing in the deep ocean. *J. Geophys. Res.*, 83:1971-1979.

Aucan, J., Merrifield, M. A., Luther, D. S. and Flament, P. (2006). Tidal mixing events on the deep flanks of Kaena Ridge, Hawaii. *J. Phys. Oceanogr.*, 36:1202-1219.

Dillon, T. M. (1982). Vertical overturns: a comparison of Thorpe and Ozmidov length scales. *J. Geophys. Res.*, 87:9601-9613.

Gregg, M. C. (1989). Scaling turbulent dissipation in the thermocline. *J. Geophys. Res.*, 94:9686-9698.

Hosegood, P., Bonnin J. and van Haren, H. (2004). Solibore-induced sediment resuspension in the Faeroe-Shetland Channel. *Geophys. Res. Lett.*, 31:L09301, doi:10.1029/2004GL019544.

IOC, SCOR, IAPSO (2010). The international thermodynamic equation of seawater – 2010: Calculation and use of thermodynamic properties. Intergovernmental Oceanographic Commission, Manuals and Guides No. 56, UNESCO, Paris, France, 196 pp.

Levine, M. and Boyd, T. J. (2006). Tidally forced internal waves and overturns observed on slope: results from HOME. *J. Phys. Oceanogr.*, 36:1184-1201.

Munk, W. (1966). Abyssal recipes. *Deep-Sea Res.*, 13:707-730.

Oakey, N. S. (1982). Determination of the rate of dissipation of turbulent energy from simultaneous temperature and velocity shear microstructure measurements. *J. Phys. Oceanogr.*, 12:256-271.

Thorpe, S. A. (1977). Turbulence and mixing in a Scottish loch. *Phil. Trans. Roy. Soc. Lond. A*, 286:125-181.

Thorpe, S. A. (1987). Transitional phenomena and the development of turbulence in stratified fluids: a review. *J. Geophys. Res.*, 92:5231-5248.

van Haren, H. (2015). Instability observations associated with wave breaking in the stable-stratified deep-ocean. *Phys. D*, 292-293:62-69.

van Haren, H. and Gostiaux, L. (2010). A deep-ocean Kelvin-Helmholtz billow train. *Geophys. Res. Lett.*, 37:L03605, doi:10.1029/2009GL041890.

van Haren, H. and Gostiaux, L. (2011). Large internal waves advection in very weakly stratified deep Mediterranean waters. *Geophys. Res. Lett.*, 38:L22603, doi:10.1029/ 2011GL049707.

van Haren, H., Laan, M., Buijsman, D.-J., Gostiaux, L., Smit, M. G. and Keijzer, E. (2009). NIOZ3: independent temperature sensors sampling yearlong data at a rate of 1 Hz. *IEEE J. Ocean. Eng.*, 34:315-322.

van Haren, H., Cimatoribus, A. and Gostiaux, L. (2015). Where large deep-ocean waves break. *Geophys. Res. Lett.*, 42:2351-2357, doi:10.1002/2015GL063329.

Winters, K. B. (2015). Tidally driven mixing and dissipation in the boundary layer above steep submarine topography. *Geophys. Res. Lett.*, 42:7123-7130, doi:10.1002/2015GL064676.